Journal of Nonlinear Optical Physics & Materials
Vol. 8, No. 2 (1999) 211–234

GUIDED-WAVE PHASE-MATCHING OF ULTRASHORT-PULSE LIGHT

C. G. DURFEE III*, A. RUNDQUIST, S. BACKUS, Z. CHANG,
C. HERNE, H. C. KAPTEYN and M. M. MURNANE
Center for Ultrafast Optical Science, University of Michigan,
2200 Bonisteel Blvd., Ann Arbor, MI 48109-2099, USA

Received 3 April 1999

We review the use of hollow waveguides for frequency conversion of ultrafast laser pulses the ultraviolet and extreme ultraviolet. Phase-matching of these processes is reached through a balance of gas and waveguide dispersion. By mixing 400 nm with 800 nm light, ultrashort (8 fs) pulses are generated near 270 nm with high efficiency $> 20\%$. Tuning of the longer-wavelength component in the mixing process allows tuning of the output from 215–308 nm. In the XUV, this guided-wave phase-matching has allowed an increase of conversion efficiency of high-order harmonic generation of 100–1000x over that obtained with a gas jet, in an experimentally-convenient geometry.

1. Introduction

Recent years have seen rapid progress in the development and characterization of high-energy ultrafast lasers with pulse duration as short as 20 fs.[1] These near-infrared sources can be used to pump optical parametric amplifiers, making it possible to generate tunable $\sim$10 fs pulses in the visible and the near infrared[2,3] regions of the spectrum. Many fields of research (solid-state physics, surface science, biophysics, reaction dynamics in chemistry[4]) would also benefit from the availability of energetic ($> \mu$J) ultrafast pulses in the deep-ultraviolet (UV). Various nonlinear-optical frequency mixing schemes have been used to generate ultrafast pulses at short-wavelengths; however, these techniques all have significant limitations. Most schemes have relied on crystalline solids as nonlinear media, where phase-matching can be accomplished using birefringence or periodic-poling.[5] These techniques are limited to wavelengths longer than ~ 200 nm by the phase-matching range allowed by the crystal.[6] Furthermore, for pulses under ~ 150 fs duration, the frequency conversion efficiency is severely limited by group velocity walkoff.

In contrast, many gases are transparent well into the vacuum ultraviolet (VUV) region of the spectrum. Shorter wavelength extreme-ultraviolet (XUV) light can propagate with moderate absorption through low-pressure gases. Furthermore, the

*E-mail: charlesd@eecs.umich.edu

reduced index of refraction of the medium greatly reduces group-velocity walkoff, making it possible to generate very short pulses. For example, we demonstrated the generation of 1 μJ, 16 fs pulses at the third-harmonic of 20 fs, 800 nm pulses focused in air or noble gases.[7] In this case, the conversion efficiency ($\sim 0.1\%$) was relatively low due to the short interaction length and poor phase-matching. One of the primary sources of phase mismatch was the intrinsic (Guoy) phase shift due to the tight focusing geometry used. Other work accomplished phase-matched frequency conversion in gases by making use of the anomalous dispersion present in narrow spectral regions in vapors[8,9] or gases[10,11] to compensate for the focusing phase shift and the normal dispersion of the gas.[12,13] The limited bandwidth of this technique makes it inapplicable to very short pulses.

Recently we demonstrated a novel approach to obtain phase-matched harmonic generation and parametric mixing in gases.[14] In this scheme, the frequency conversion takes place in a gas-filled hollow waveguide. The use of a waveguide increases the interaction length at high intensity and eliminates the focusing phase shift. In the guided-wave phase-matching technique, the dispersive contribution from the waveguide is balanced with the pressure-dependent dispersion of the gas to phase-match the conversion process. The nonresonant nature of this phase-matching process allows the generation of sub-10 fs pulses in the UV.

Section 2 will describe the principles behind guided-wave phase-matching and how the propagation phase of a beam can be controlled when it is guided in a gas-filled capillary. Sections 3 and 4 review the phase-matching considerations and experimental results for generation of ultrashort pulses in the UV and the XUV, respectively.

2. Hollow-Core Waveguides for Phase-Matching

It has long been recognized that nonlinear optical effects are often best studied and exploited in a guided-wave geometry. Soliton pulse propagation, and various guided-wave electro-optic modulation techniques[15] are outstanding examples of this. However, solid optical fibers have limited use for $\ll 1$ ps duration pulses because of the strong linear dispersion of the material, and because of damage at high peak intensity. Hollow waveguides can alleviate these problems, and have also been used for nonlinear-optics. For example, glass or fused-silica capillaries have been used to increase the conversion efficiency of Raman generation in gases.[16] (Raman generation is a self-phase matched process.) More recently, capillary waveguides have been used to broaden the spectrum of an intense ultrashort pulse through self-phase modulation.[17] Recompression of these pulses can result in sub-10 fs-duration light pulses with high (microjoule to millijoule) pulse energy.[18] Other experiments have attempted to use capillary waveguides to implement anomalous-dispersion phase-matched conversion into the VUV, with marginal results.[19]

However, none of this past work has made use of the waveguide to alter the propagation and phase-matching conditions of the process, despite the fact that

this "modal" dispersion is quite well-known.[20] The guiding of the interacting waves introduces a source of modal phase that provides an extra adjustable parameter. In our experiments, we demonstrate that this can be exploited in harmonic generation and frequency mixing of ultrafast pulses.

2.1. *Propagation Phase for a Gas-Filled Hollow Waveguide*

Hollow-core waveguides differ significantly from conventional optical fibers. In solid-core optical fibers, light is guided by total internal reflection or refraction, and loss in the fiber depends primarily on absorption of the beam by the host material. In contrast, hollow dielectric waveguides guide laser beams through Fresnel reflections at the inner wall of the capillary. The mode structure is calculated by solving the radial wave equation. The mode-structure is similar to that of a step-index optical fiber, with some modifications near the walls to satisfy the boundary conditions.[20,21] The lowest-order mode profile in a capillary waveguide of radius a is the linearly polarized EH_{11} hybrid mode, with $E(r) \approx E(0)J_0(k_T r)$ and a transverse wavenumber $k_T = u_{11}/a$, where $u_{11} = 2.405$ is the first zero of the Bessel function J_0. Figure 1(a) shows the field profiles of the first three radial hybrid modes (EH_{11}, EH_{12}, EH_{13}). Losses from the Fresnel reflections result in attenuation of the guided modes. The field loss rate α for the hybrid modes is[20]

$$\alpha = \left(\frac{u_{nm}}{2\pi}\right)^2 \frac{\lambda^2}{a^3} \mathrm{Re}(\nu_{EH}^2), \tag{1}$$

where u_{nm} is the modal constant for azimuthal and radial modal indices m and n. The material index of refraction enters into Eq. (1) through the constant $\nu_{EH} = (\nu^2 + 1)/[2(\nu^2 - 1)^{1/2}]$, where ν is the ratio of the refractive index of the capillary material to that of its contents. The strong modal dependence of the losses can be used to simulate single-mode propagation by proper selection of the capillary length so that it transmits approximately 60% of the lowest-order mode (see Fig. 1(b)). The attenuation is much greater for longer wavelengths. For example, beams propagating in the lowest order mode (EH_{11}, $u_{11} = 2.405$) of a waveguide with core radius $a = 75$ μm and length 1 m, the intensity losses at wavelengths 800 nm, 400 nm and 267 nm, are 52%, 85%, and 93%, respectively. Since the guided mode has very little energy inside the capillary wall, absorption of the guided light by the wall material has no effect on the transmission.

By countering diffractive spreading of a wave, a waveguide adds a geometrical component to its wavevector. For a hollow dielectric waveguide filled with a homogeneous medium of refractive index n, the longitudinal propagation constant, k, is given by $k^2 = n^2 k_0^2 - k_T^2$, where k_0 is the vacuum wavenumber. The propagation constant is therefore given by

$$k = \frac{2\pi n(\lambda)}{\lambda}\left\{1 - \frac{1}{2}\left(\frac{u_{nm}}{2\pi}\frac{\lambda}{a}\right)^2\left[1 + \mathrm{Im}\left(\frac{\nu_{EH}\lambda}{\pi a}\right)\right]\right\}. \tag{2}$$

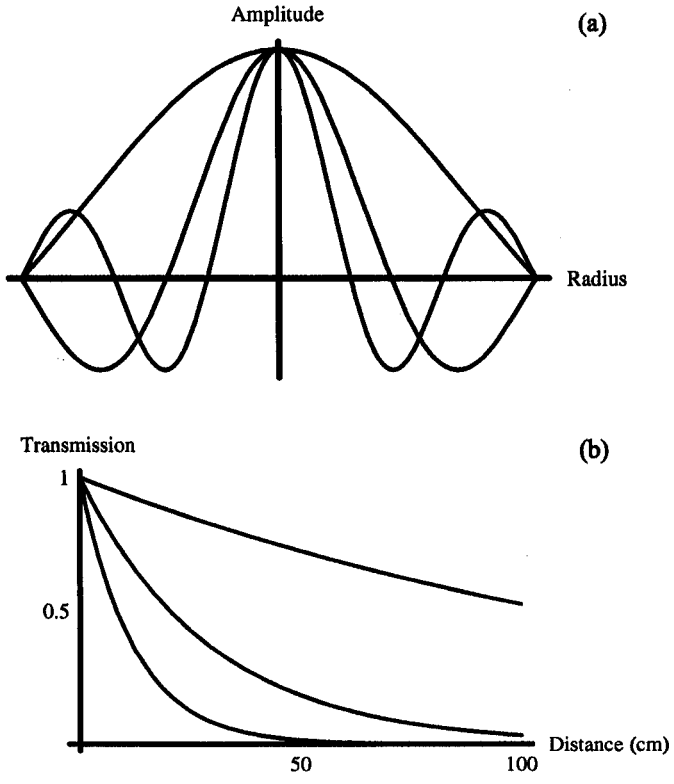

Fig. 1. (a) Field profiles for the first three radial modes of a capillary waveguide; (b) Power transmission vs. capillary length for these three modes (capillary diameter 150 μm).

The last term of Eq. (2) corresponds to the contribution of the wall material absorption to the propagation phase and is generally negligible as it scales as λ/a. The index of refraction for a partially ionized gas may be written in the form $n(\lambda) = N_a\delta(\lambda) - N_e r_e \lambda^2/2\pi$, where N_a is the atomic density, $\delta(\lambda)$ contains the gas dispersion information, N_e is the electron density and r_e is the classical electron radius. Equation (2) may be expressed in approximate form as

$$k(\lambda) \approx \frac{2\pi}{\lambda} + \frac{2\pi N_a \delta(\lambda)}{\lambda} - N_e r_e \lambda - \frac{u_{nm}^2 \lambda}{4\pi a^2}. \tag{3}$$

The propagation constant is the sum of four sources of dispersion: vacuum, gas, free-electron and waveguide.

2.2. *Intensity-Dependent Effects*

One advantage of using hollow waveguides for ultrafast nonlinear optical experiments is that the intensity at the center of the waveguide can far exceed the damage threshold of the waveguide material. The intensity in the walls is much lower than at the center, and peak intensities in the 10^{15} W/cm^2 range can be guided without

damage to the walls.[22] At high intensity, both the nonlinear refractive index and the ionization of the gas affect the propagation. In an unrestricted medium, these two effects lead to self-focusing and self-defocusing, respectively. Guiding permits higher pulse intensity without adverse changes to the guided mode.[23] Moreover, provided the guided beam propagates for several Rayleigh ranges, the nonlinear phases experienced by the different intensity portions of the beam are distributed throughout the mode.

This modal averaging means that Eq. (3), which assumes the ionization is equally distributed across the mode, overestimates the influence the effect of the free electrons on the propagation constant when the guided beam produces the ionization. In this case, the ionization is localized near the optical axis, so only a portion of the fundamental mode propagates through the plasma. Figure 2(a) shows

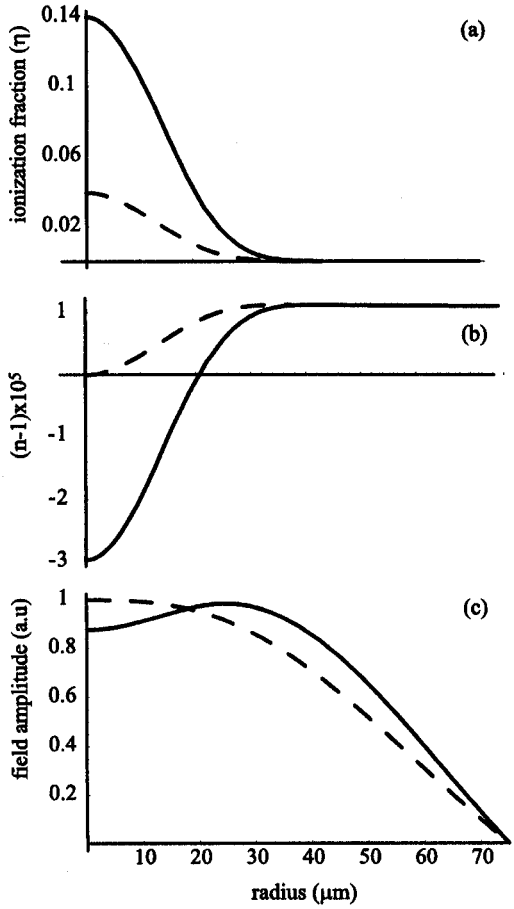

Fig. 2. (a) Calculated radial ionization profiles at the peak of a 20 fs pulse in argon for a peak intensity of 1.6×10^{14} W/cm^2 (dashed) and 2.0×10^{14} W/cm^2; (b) Resulting radial refractive index profile at an ambient pressure of 20 Torr; (c) Calculation of the radial field profiles for these two intensities.

the ionization profile $\eta(r)$ at the peak of a 20 fs pulse for two intensities (1.6×10^{14}, 2.0×10^{14} W/cm^2) irradiating argon. Figure 2(b) shows the refractive index profile $n(I,r) = 1 + N_a\delta(\lambda) - N_e(r)r_e\lambda^2/2\pi + n_2I(r)$ for these two cases, while Fig. 2(c) shows the lowest-order fields calculated by numerically solving the radial wave equation. When the nonlinear refractive index and the plasma refractive index are both sufficiently small, the shape of the guided mode field is not greatly affected. In this regime, the variations in the radially-dependent refractive index, may be treated as a perturbation, in a approach similar to that taken with self-phase modulation in optical fibers.[15] Specifically, we can calculate a new effective refractive index, $n_{\text{eff}}(I)$, by averaging across the fundamental mode

$$n(I) = \frac{\int J_0(k_T r)\eta(I,r)rdr}{\int J_0(k_T r)rdr}. \tag{4}$$

The modal averaging reduces the effect of the plasma density on the propagation constant by as much as a factor of five. In the limit of a high density and/or a large degree of ionization, both the modal field profile and its propagation constant must be calculated either by solving the transverse wave equation or, more generally, by calculating the transient beam propagation through the waveguide.

3. Phase-Matched UV Generation

Most efforts at frequency conversion in gases have made use of a focused-beam geometry. In that geometry, the wavefront changes curvature as it passes through the focus, leading to the Guoy phase-shift[24]: $\phi = \tan^{-1}(z/z_0)$, where $z_0 = \pi w_0^2/\lambda$ is the Rayleigh range of the focused beam. The problems associated with the Guoy phase-shift in odd-harmonic generation have been well documented.[10,12] In the perturbation limit, harmonic light is expected to be seen only with negative phase mismatch ($\Delta k = k_q - qk_1$); otherwise, harmonic light generated in the half-space before the focal point is cancelled by the light generated after it. The negative phase mismatch can be created experimentally by the use of an anomalously dispersive medium[8] or through difference-frequency mixing.[13] A half-space[12] or a gas jet may also be used to mitigate this effect.

For a beam propagating as spatial mode of a waveguide, however, the phase of the wavefront evolves linearly with propagation distance. This propagation phase is normally dispersive, but through the mixing of light propagating at different frequencies and/or in different spatial modes[15,25,26] phase-matching can be achieved, and the signal can build up over a long interaction length. Near-resonant phase-matching with a capillary waveguide was proposed[27] and tested,[19] but the contribution of the waveguide phase was not accounted for. In the experiment, molecular absorption limited the efficiency ($< 10^{-3}$). More important, the intrinsic bandwidth limitations of this technique limit its usefulness for frequency conversion of ultrashort pulses.

In the following sections, we describe the guided-wave phase-matching technique for conversion to the deep-UV. In this wavelength regime, noble gases are normally

dispersive. There are two options for phase-matching the third-order process: direct third-harmonic generation or parametric amplification ($\omega_{signal} = 2\omega_{pump} - \omega_{idler}$). In the former case, the output is placed in a higher spatial mode.[28] In the latter, all the interacting beams can be in the lowest spatial mode, resulting in better signal/nonlinear polarization overlap and better conversion efficiency.

3.1. *Guided-Wave Phase-Matching*

First consider the process of qth harmonic generation of a pump beam at central frequency ω_1 propagating in the capillary waveguide, $\omega_q = q\omega_1$. Neglecting sources of nonlinear phase, the phase mismatch, $\Delta k = k_q - qk_1$ may be written as

$$\begin{aligned}\Delta k &= \Delta k_{mat} + \Delta k_{mode} \\ &= \frac{2\pi N_a}{\lambda_q}\left(\delta(\lambda_q) - \delta(\lambda_1)\right) - \frac{\lambda_q}{4\pi a^2}\left(u_q^2 - q^2 u_1^2\right), \end{aligned} \tag{5}$$

where u_1 and u_q are the modal constants for the fundamental and the harmonic beams. The phase mismatch results from a modal dispersion term ($\Delta k_{mode} \propto 1/\pi a^2$) minus a material dispersion term ($\Delta k_{mat} \propto N_a$). For harmonic light in a spectral region that is normally dispersive for the gas, $\Delta k_{mat} > 0$. Without the waveguide, the phase velocity of the harmonic would be too slow; by placing the harmonic in a higher spatial mode, the phase velocity can be increased (i.e., so that $\Delta k_{mode} > 0$). This imposes the following condition on the harmonic mode $u_q > qu_1$. For example, if the fundamental is in the lowest order mode ($u_1 = u_{11} \approx 2.405$), then for $q = 3$, the lowest spatial mode for the harmonic will be $u_3 = u_{13} \approx 8.654$. When $u_q > qu_1$, the pressure can be adjusted to reach the phase-matched condition $\Delta k = 0$.

The primary limitation of the conversion efficiency in this case is the poor overlap between the harmonic spatial mode and the nonlinear polarization. The buildup of the nonlinear signal depends on the net in-phase contribution of the nonlinear polarization induced by the driving pulse to the generation of a signal wave with a different spatial mode. The overlap between the field profile of the signal field ψ_s with that of the input beams ψ_1, ψ_2, ψ_3 can be expressed in terms of an effective area[25]

$$\frac{1}{A_{eff}} = \frac{\int_0^{2\pi}\int_0^{\infty} \psi_s\psi_1\psi_2\psi_3 r dr d\theta}{D_s^{1/2} D_1^{1/2} D_2^{1/2} D_3^{1/2}}, \tag{6}$$

where D_m ($m = s, 1, 2, 3$) are the normalization factors for the mode profiles,

$$D_m = \int_0^{2\pi}\int_0^{\infty} |\psi|_m^2 r dr d\theta. \tag{7}$$

The effective area for all beams in the lowest order mode corresponds very closely to the area within the 1/e radius of that mode. For the case of conversion into the EH_{13} mode, the value of this overlap integral is 2.3% of this value. This can be compensated to some extent with an increase in the length of the waveguide. However,

the maximum useful length is limited by two factors: (1) the phase-matching bandwidth (which decreases with increasing propagation length), or (2) the propagation loss of either of the beams.

Sum-difference frequency mixing, rather than simple harmonic generation, makes it possible to obtain phase-matched conversion with all colors in the same waveguide mode, dramatically increasing the spatial overlap and the conversion efficiency of the process. Consider the general case of difference frequency mixing using two colors in the capillary waveguide, at central frequencies ω_1 and ω_2. The phase mismatch for difference frequency mixing, $\omega_3 = N\omega_2 - M\omega_1$, is $\Delta k = k_3 + Mk_1 - Nk_2$, or

$$\Delta k = 2\pi N_a \left(\frac{\delta_3}{\lambda_3} + \frac{M\delta_1}{\lambda_1} - \frac{N\delta_2}{\lambda_2} \right) - \frac{1}{4\pi a^2} \left(\lambda_3 u_3 + M\lambda_1 u_1 - N\lambda_2 u_2 \right). \quad (8)$$

Here, the order M and the wavelength λ_1 can be chosen so that $\Delta k_{mode} > 0$ with all beams in the lowest-order spatial mode (i.e., $u_1 = u_2 = u_3 = u_{11}$). For the particular case where $\lambda_1 = 2\lambda_2$, and $u_1 = u_2$, $\Delta k_{mode} > 0$ for any signal mode. In experiments thus far, the second-harmonic of Ti:sapphire (at 400 nm) has been used as the short-wavelength pump; for the second "idler" color, light at the Ti:sapphire fundamental (800 nm) and light from a conventional optical parametric amplifier (tunable throughout the infrared) have been used (allowing tuning of the output through the UV).

3.2. *Experimental Method and Results*

These experiments used a kilohertz repetition-rate, two stage multipass Ti:sapphire amplifier system (< 20 fs, 4.5 mJ)[29] developed in our laboratory. Pulses of 0.5–1 mJ are down-collimated and frequency-doubled in a nonlinear crystal (see Fig. 3). This blue pump pump light and near-IR idler light are then recombined using a dichroic mirror (after adjusting the polarization and the time-delay of the pulses to coincide). The two collinear beams are then focused together using a curved Al-coated mirror into a capillary of $\sim$100–200 μm inside diameter, enclosed in a gas cell. The cell uses thin (250 μm) sapphire windows, and is evacuated and filled with gas to a pressure that gives the optimum conversion efficiency. After filling, the gas does not normally need replenishment.

The preliminary experiments studied simple third-harmonic generation into higher-order spatial modes. With the fundamental coupled to the EH_{11} mode of the capillary (153 μm core diameter, 30 cm length), output to the EH_{13} mode should be phase-matched at an optimum pressure of $p_{opt} = 60$ Torr of krypton (using Eq. (5) and the dispersion formulae given by Dalgarno and Kingston[30]). For this capillary, the ideal transmission of 800 nm light was 83%, while the measured value was 46%. As the throughput of a TEM_{00} HeNe laser beam was only 10% less than ideal, the imperfect transmission of the 800 nm light likely results from imperfect mode-matching into the fiber. The UV output of the fiber was separated from the fundamental a series of dichroic mirrors with a 30 nm bandwidth centered

at 270 nm, with a bandwidth of 30 nm. The beam was then observed using a CCD spectrograph or, after passing through a fused silica prism to further reject the 800 nm light, a calibrated photodiode power meter (Newport 818-UV detector).

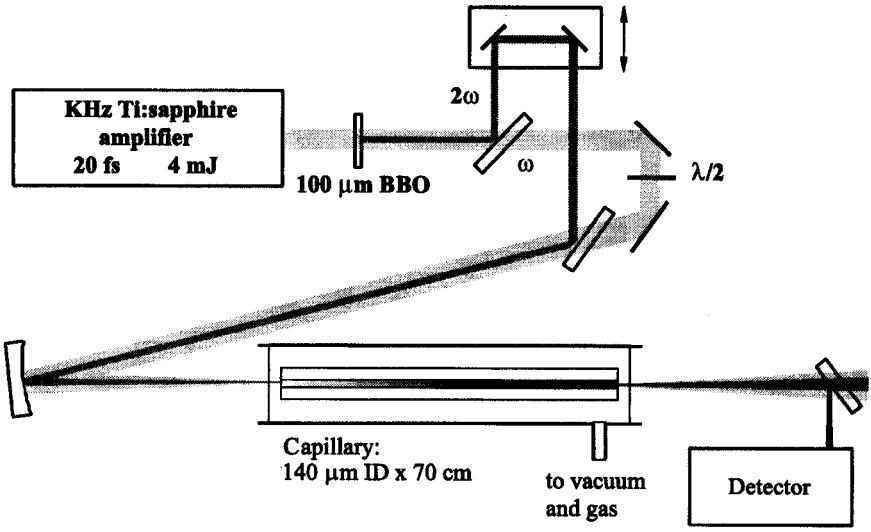

Fig. 3. Experimental layout for the UV generation experiments.

Figure 4 shows the 3ω signal versus pressure using krypton in the cell. The output energy shows a clear maximum at 55 Torr, in good agreement with the value (60 Torr) calculated for phase-matching to the EH_{13} mode. The measured bandwidth was 8 nm. This matches well the spectral width of $\Delta\lambda_3 = \Delta\lambda_1/n^{3/2}$ predicted by perturbation theory for Gaussian pulses: for $\Delta\lambda_1 = 40$ nm, $\Delta\lambda_3 = 8$ nm. This shows that the process is phase-matched over the entire pulse bandwidth. Using 250 μJ of 800 nm input, the output energy of the UV pulse was measured to be 0.28 μJ, giving an efficiency of 0.2% (assuming 145 μJ actually enters the waveguide). This compares favorably with the case of third-harmonic generation by a tight focus in air.[7]

Increasing the interaction length in this setup would restrict the phase-matching bandwidth, so to improve the conversion efficiency, it was necessary to do the sum-difference frequency mixing to improve the overlap between the modes of the interacting beams. In these experiments, the fundamental and the second harmonic were coupled to the lowest-order spatial mode of a capillary (127 μm core diameter, 60 cm long), yielding output at 267 nm in the same (EH_{11}) spatial mode. The divergence of the input telescope was adjusted to optimize the coupling of the 400 nm light (35% throughput); the fundamental beam was not as well optimized ($< 10\%$ throughput). Figures 5(a) and 5(b) shows the UV output pulse energy as a function of argon and krypton gas pressure. The positions of the peaks are in excellent agreement with the values calculated from Eq. (5). The

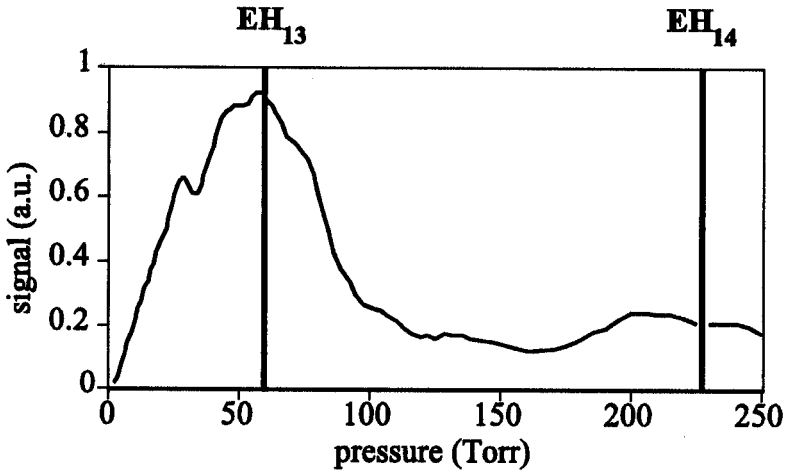

Fig. 4. Third harmonic signal versus pressure of krypton in the cell. Reference lines indicate the calculated optimum pressure for conversion to the radial modes shown.

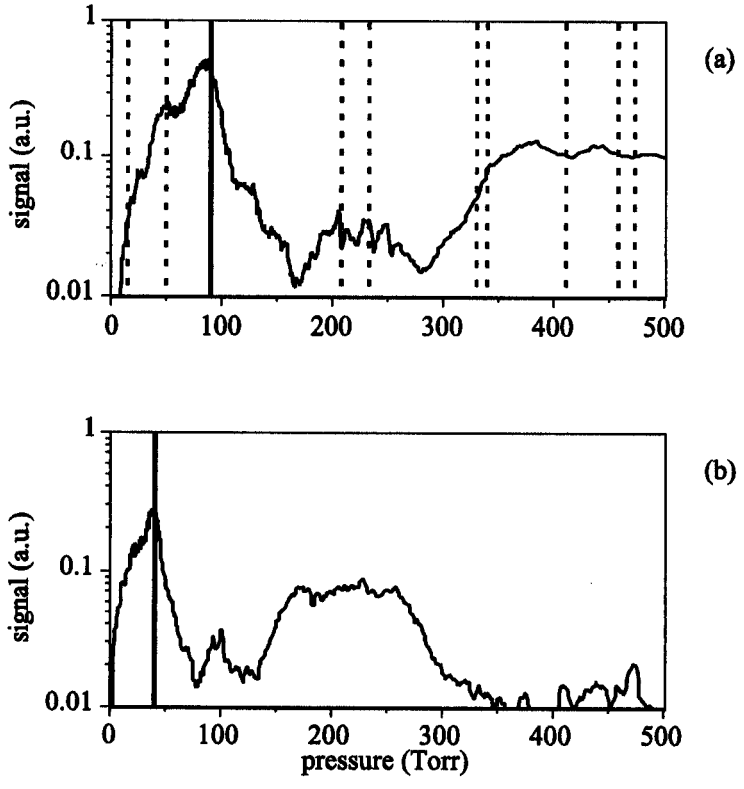

Fig. 5. Mixing yield near 267 nm versus argon (a) and (b) krypton gas pressure in a capillary 127 μm in diameter and 60 cm in length. The solid reference lines show the calculated optimum pressure for conversion to the lowest order mode. The dashed reference lines in (a) show the optimum pressure for other mode combinations.

measured (calculated) output energy shows a clear maximum at 85.1 (89.7) Torr for argon and 38.9 (39.2) Torr for krypton. For these conditions, the output mode is very nearly Gaussian, since the EH_{11} mode closely-corresponds to a Gaussian beam in free space. The pressure tuning curves also show low secondary peaks. These correspond to conversion with other combinations of spatial modes for the pump, signal, and idler that can phase-match, but with a smaller spatial overlap. The pressure-tuning curve for krypton is similar in structure to that for argon, after scaling the pressure axis according to the dispersion of the two gases. This is a good indication that this structure is a result of the geometry of the waveguide, rather the particular characteristics of the gas. In conditions where 30 μJ of 400 nm energy and 64 μJ of 800 nm energy passed through the fiber, the output energy at $\sim$267 nm was 4 μJ, corresponding to a 13% conversion of 2ω to 3ω. In this case, the large conversion efficiency and the substantial average power of this beam allowed us to use a standard thermal power meter to measure the power, rather than a photodiode. In later experiments, we have increased the conversion efficiency to $>20\%$ of the blue pump, by using a better quality capilliary and increasing the area of the capillary by 25%. In this case, the output was $>$ 10 μJ at 267 nm.

The low dispersion of gases results in an extremely low group velocity walkoff (<6 fs) and allows for the generation of very short pulses in the UV. However, the strong dispersion of air and all optical materials in the UV makes it necessary to use a pulse compressor to obtain the shortest pulse duration at the point of measurement. For example, an 8 fs pulse at 266 nm will broaden to 24 fs after propagating through just 1 m of air. Recently, we have shown that by compressing the UV output of the capillary, 8 fs pulses can be generated at 270 nm.[31] After collimation of the output of the capillary, the UV pulse was directed to a dual-grating pulse compressor (300 gr/mm, 300 nm blaze, Al coating). To minimize the losses in the grating compressor, we used a single-pass configuration, resulting in a throughput of 50%. Using a novel layout for a self-diffraction frequency-resolved optical gating measurement, the pulse was fully characterized (see Fig. 6). These 8 fs pulses are the shortest generated and measured in the UV to date. The pulses are actually shorter than expected owing to cross-phase modulation of the UV spectrum by the strong IR pulse. With higher intensity and proper compression, production of pulses in the 3 fs range should be possible.

The mixing process allows the production of pulses tunable throughout the deep-UV by using a variable idler wavelength. With the signal and idler, and their second harmonics, our optical parametric amplifier (Spectra-Physics) has a tuning range that spans the range of at least 590–2600 nm, giving a tuning range (with 400 nm pump pulses) of 217–305 nm. For each wavelength (see Fig. 7), the pressure of the gas (argon) was readjusted to maintain the proper phase-matching condition. The output energy in each case was $\approx$ μJ or greater. Improvement of the beam coupling will increase the output. Guided-wave phase-matching may also be extended to shorter wavelengths in the VUV range through higher-order mixing. The spectrum centered at 200 nm in Fig. 7(a) resulted from a six-wave mixing process: $\omega_{signal} =$

$3\omega_{pump} - 2\omega_{idler}$ (where second harmonic and the fundamental were used as the pump and idler, respectively). The broadening of the spectrum in this case resulted from self-phase modulation of the 800 nm light.

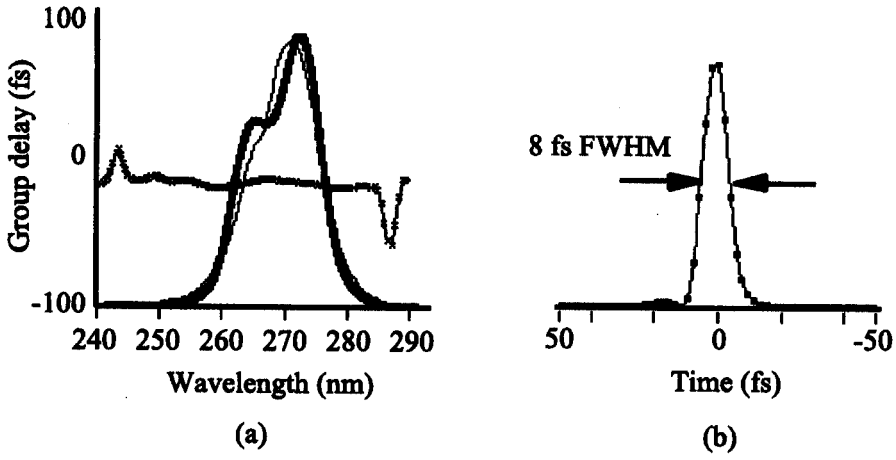

Fig. 6. (a) Measured spectrum (thick line), deconvolved spectrum (thin line) and deconvolved group delay for a pulse compressed to 8 fs; (b) Deconvolved temporal intensity profile.

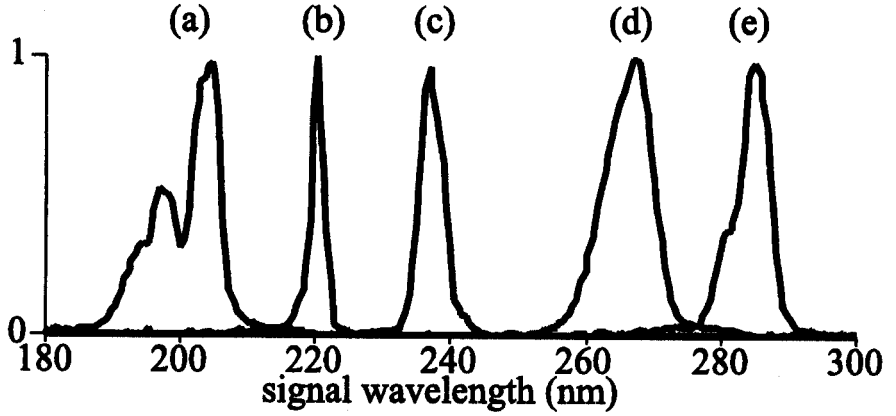

Fig. 7. Mixing output spectra for high-order mixing in a capillary waveguide filled with argon. (a) six-wave mixing (3ω (400 nm) – 2ω (800 nm)); (b)–(e) four wave mixing (2ω (400 nm) – ω_{idler}), with idler wavelengths 2200 nm, 1280 nm, 800 nm and 670 nm respectively.

4. Phase-Matched High-Order Harmonic Generation

In recent years the technique of high-harmonic generation (HHG) has proved to be a useful source of XUV and soft x-ray light.[32,33] In the process of high-harmonic generation an atom illuminated by light of ionizing intensity radiates coherent harmonics

of the incident laser that extend into the soft-x-ray region of the spectrum.[33–41] This process is of interest both in basic and applied science. From a fundamental physics point of view, HHG explores the boundaries between classical and quantum behavior. It is also a practical coherent ultrafast radiation source in the VUV and soft-x-ray regions of the spectrum. The use of very short laser pulses has been shown to produce coherent light to wavelengths below 3 nm.[41,42] Furthermore, HHG is the most likely method for generating sub-femtosecond pulses[40,43,44] Despite the low efficiency of this process ($< 10^{-8}$ conversion of laser light into one harmonic peak), the photon flux generated is still sufficient to be useful for some applications in ultrafast x-ray spectroscopy. However, significantly more applications would be possible with the highest possible conversion efficiency of laser light to x-rays. Thus in its application as a coherent light source, it would be desirable to phase-match the conversion process. This conversion efficiency depends both on the fundamental laser-atom interaction, i.e., the high-order nonlinear-optical susceptibilities, and on the buildup of the signal electromagnetic wave over an extended interaction length containing many atoms.[35,45] In the case of the nonlinear susceptibilities, there is a tradeoff between the magnitude of the susceptibility and the highest, "cutoff" harmonic order, which is related to the ionization potential of the atom. Molecular and cluster species have also been investigated for high-harmonic generation as a means of obtaining higher susceptibilities than in ordinary atomic systems.[46]

Most experiments in high harmonic generation to date have been done in the tight focusing geometry, where the phase shift due to the laser focus dominates and limits phase-matching. Although proper choice of focusing conditions can improve the coherence length, the useful interaction length is still fundamentally limited by the laser beam divergence. Macroscopic propagation effects play a dramatic role in the observed signal intensity. In past work, HHG was implemented by focusing an intense femtosecond-duration light pulse into a gas cell or jet.[35,45,47] This work has shown that the relative phase shift of the various interacting waves as they pass through the focus (i.e., the Guoy phase shift) has a very significant effect on the signal intensity. By positioning the interaction region after the focus of the beam, this phase shift can be used to enhance the coherence length of the interaction.[32,48] However, the divergence of the laser beam and the nonlinearity of the propagation phase with the axial distance in this case inherently limit the interaction length, or require a large confocal parameter (and large laser energy) to implement efficiently.

Recently we have demonstrated that the guided-wave phase-matching technique may be extended to the phase-matching of these high-harmonics, thereby circumventing this limitation.[49,50] In this case, the neutral gas is anomalously dispersive for harmonic generation, and can be used to directly counter the normal dispersion of the waveguide and free electrons.[14] By adjusting the gas pressure within the waveguide to tune the phase velocity of the fundamental, phase-matched conversion of 800 nm light to wavelengths around 25 nm was demonstrated in argon, resulting in an increase in efficiency of 100–1000x over that found in the gas jet geometry for the same harmonics.

4.1. *High-Order Phase-Matching Considerations*

For HHG, there are several important differences in the guided-wave phase-matching process. First, the neutral gas absorbs the harmonic signal — this limits the interaction length to approximately the absorption depth. Second, since this restriction limits the capillary length, and the harmonic wavelength is so short, the harmonic light effectively does not encounter the walls of the waveguide. Finally, the HHG process is related to the ionization process, and the free electron dispersion leads to qualitatively new regimes of phase-matching.

For photon energies ε_{phot} lower than that of the first excited state, the contribution $N_a\delta$ to the refractive index is positive ($\approx +3 \times 10^{-4}$, for 1 bar of Ar, $\lambda = 0.8$ μm) while for $\varepsilon_{phot} > I_P$, it is negative (-1×10^{-4}, for $N = 27$). This anomalous gas dispersion gives $\Delta k_{mat} < 0$ in Eq. (5), and allows phase-matching with $\Delta k_{mode} < 0$. In terms of phase-velocities: the fundamental propagates at velocities less than c, while the harmonics propagate at phase velocities slightly higher than c. The presence of the waveguide speeds up the fundamental with respect to the harmonic, and the precise phase-velocity for phase-matching can be achieved by tuning the gas pressure. This regime of phase-matching works well for very low levels of ionization.

An important consideration in the phase-matched generation of light with $\varepsilon_{phot} > I_P$ is absorption of the signal. Argon, for example, has a transmission window over the range 40–100 eV. In the presence of absorption, the equation for the growth of the signal wave can be written as

$$\frac{dE}{dz} \approx -\alpha E + iN_a\chi_{eff}^{(q)}E_0^s e^{-i\Delta kz}\,, \tag{9}$$

where α is the field absorption coefficient, s is the effective field dependence of the nonlinearity. (~ 5[35]). For a constant axial density profile, this has the solution

$$|E|^2 \approx N_a^2|\chi_{eff}^{(q)}E_0^q|^2\left(\frac{1+e^{-2\alpha L}-2e^{-\alpha L}\cos\Delta kL}{\alpha^2+\Delta k^2}\right) \tag{10}$$

which reduces to the familiar $\mathrm{sinc}^2(\Delta kL/2)$ dependence for $\alpha = 0$. The important physical consequence of Eq. (10) is that the signal strength is determined by the shorter of the coherence length and the absorption depth, $l_{abs} = 1/2\alpha$. The strong absorption of gases for photon energies greater than the ionization potential therefore dominates the yield that can be obtained at different harmonics.[51,52] As phase-matching is extended to higher orders or more complicated geometries,[53] or using wave-mixing schemes,[54] this limitation can be circumvented by operating in the transparency regions of the various gases.

4.2. *Experimental Method and Demonstration of Phase-Matching*

For these experiments,[49,50] pulses from the kilohertz laser system described above were focused with a fused silica lens were focused into a 150 μm inner-diameter

capillary waveguide (see Fig. 8). A three-segment capillary tube (6.3 mm outer diameter) was used for these experiments.[49,51] A constant gas pressure is held in the main, center capillary by using two short capillary sections sealed on their perimeter with o-rings at either end to restrict the gas flow out into the vacuum system. The three sections are all clamped into a V-groove to ensure the alignment of the bores. The separation of the capillary lengths was kept to < 0.5 mm to ensure little loss in transmission. The total capillary length was 6.4 cm, with a central section length of 3 cm. At the input, this arrangement avoids ionization defocusing at high input intensity; at the output, it avoids excessive absorption of the harmonic signal by the neutral gas. The system gas load is greatly reduced compared with a pulsed jet operating a high repetition rate.

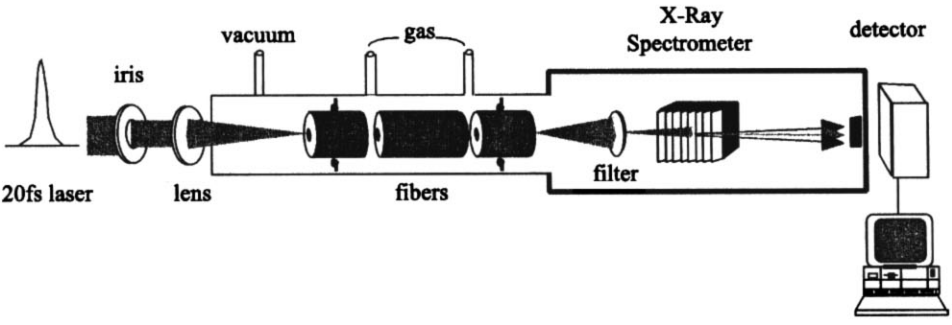

Fig. 8. Experimental setup for the generation of phase-matched high-order harmonics.

Mode-matching of the beam into the lowest spatial mode was critical in these experiments. Phase-matching in this experiment is sensitive to the propagation mode of the fundamental, and owing to the high degree of nonlinearity of the ionization process, spatial mode beating could result in a non-uniform axial intensity profile. Unlike the experiments described above, where the waveguide itself was aligned to the beam, the orientation of the waveguide was determined by entrance of the spectrometer. Therefore mode-matching was accomplished by manipulating the position and direction of the input beam. The position of the focal spot was optimized with a 3-axis translation stage for the lens. The approach angle of the beam to the fiber was controlled by translating the beam before the lens with a parallel mirror pair mounted on a tilt platform. An iris centered on the input beam was used to fine-tune the focal spot diameter to match that of the lowest order mode of the waveguide ($\sim 66\%$ of the capillary diameter). A mirror within the vacuum chamber could be inserted to direct the beam out of the chamber, so that the mode quality and the transmitted power could be observed while making adjustments to the fiber coupling under operating conditions.

An aluminum filter (0.2 μm) rejected the fundamental and passed light in the 11–45th harmonic range (17–70 eV). The harmonic spectrum was dispersed using an imaging grazing-incidence spectrometer (Hettrick Hi-Refs SXR-1.75) and detected

using and imaging microchannel plate pair coupled to phosphor screen. The image was either viewed with a CCD camera/frame capture system, or the signal level from a single peak could be detected using a photomultiplier tube coupled to a boxcar integrator. In other experiments, the spectrometer was removed, and the harmonic beam was directly observed using the microchannel plate detector (to inspect the harmonic beam profile) or an x-ray diode (to estimate the absolute yield).

If phase-matching of conversion of laser light into x-rays is achieved, we should observe a dramatic increase in x-ray output at the optimum pressure for a given harmonic order. Figure 9 shows the pressure dependence of the measured yield (normalized) for argon. At high pressures there is neither absorption nor distortion of the fundamental; the decrease in signal at high pressures is due to phase mismatch. By measurement of the signal with the x-ray diode we estimate a conversion efficiency in argon of 10^{-5}–10^{-6}, with approximately 0.5 nJ into each of 5 harmonics centered on the 29th order. The optimum phase-matching pressure for each harmonic is slightly different, because the higher harmonics are generated at higher values of ionization.

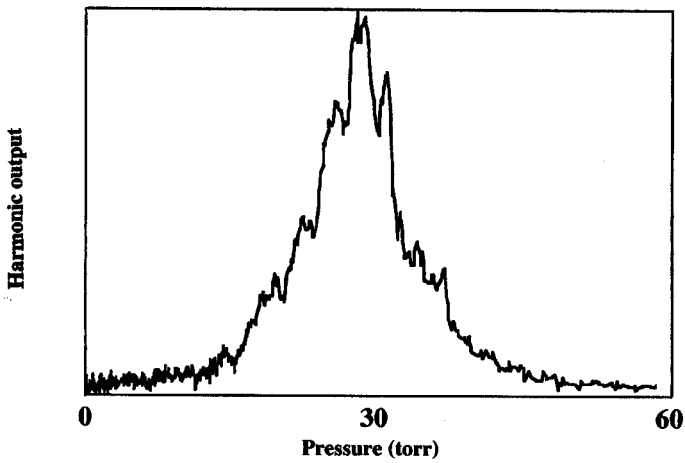

Fig. 9. Yield of the 29th harmonic (27 nm) versus argon pressure.

The harmonic yield is strongly influenced by absorption by the neutral gas. Figure 10 shows the transmission profile of argon, and the measured harmonic signal for a peak intensity of 1.9×10^{14} W/cm^2. Here, the signal for harmonic orders below the 23rd was greatly attenuated because of strong absorption in the argon gas. As the harmonic order increases, the gas transmission increases, giving rise to a strong signal from the center section, where the constant pressure allows a phase-matched signal to build up over a long distance. The decrease in the signal with increasing harmonic order beyond order 29 results from the normal cutoff at this intensity. The strong correlation of the harmonic yield with the transmission profile of the gas is evidence that the signal is being generated over a long interaction length.

This data sharply contrasts to the usual plateau of harmonics, and shows clearly that the phase-matching allows the signal strength to be limited by the absorption depth. Clearly, relatively high transmission within the neutral gas is essential for high conversion efficiency. The use of short input pulses allows the transmission window of argon to be reached without excessive ionization.

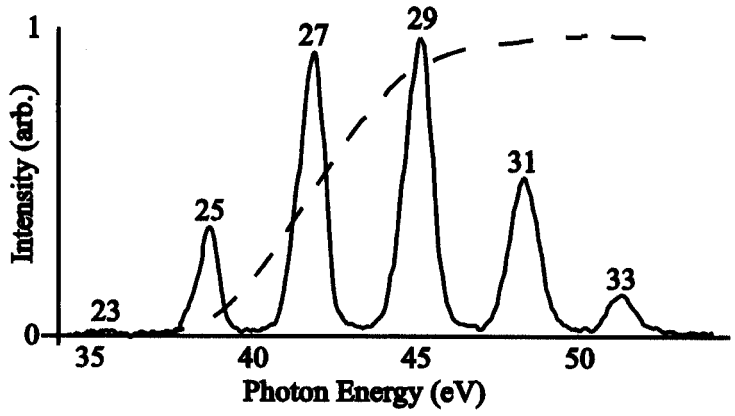

Fig. 10. Measured harmonic spectrum at 1.8×10^{14} W/cm^2 (solid) and the calculated transmission of 5 mm neutral argon at 30 Torr.

4.3. *Regimes of Phase-Matching*

We have observed that there are several regimes of phase-matching. In the limit of small fractional ionization, the neutral-gas and the waveguide dispersion balance one other. This regime is similar to that found above for the generation of UV light, except that the anomalous dispersion of the gas allows for the phase-matching of direct harmonic generation without the need for difference-frequency mixing. For a higher ionization fraction, the free electron dispersion dominates that of the waveguide, resulting in an optimum pressure that is very sensitive to the level of ionization, and therefore sensitive to the absolute phase of the carrier wave with respect to the pulse envelope. Finally, in regions of positive phase mismatch, off-axis (Cerenkov) phase-matching is observed.[50]

The first phase-matching regime, in which there is a dispersive balance between the neutral gas and the waveguide, can be observed with a low level of incident laser intensity (to minimize ionization). Figure 11 shows the dependence of the harmonic signal (harmonics$^{19-23}$) on the pressure of argon, at an intensity of 1.2×10^{14} W/cm^2 (140 μJ, 23 fs). At this intensity, cutoff harmonic is the 25th, and the ionization fraction at the peak of the pulse is 0.5%. The curves show two peaks: the low-pressure peak results from conversion within the central, constant density section of the cell. As there is very little ionization, the optimum pressure is at $\sim$15 Torr, as predicted by theory. The 23rd harmonic is produced in the presence of ionization,

and is therefore broadened and shifted to higher pressure. The high-pressure peaks in Fig. 11 result from conversion within the last section of the capillary cell. The pressure drops (~ 3x) in this section as the gas accelerates into it.[55] Within the end section, the pressure drop as a function of position is given by $P(z) = (P_{in}^2 - \kappa/z)^{1/2}$, where P_{in} is the input pressure, and κ is the throughput per unit length, a function of the capillary diameter and the gas viscosity. Within the density gradient, the propagation phase follows the equation $d(kz)/dz = k_0 n(z)$. Owing to this variable propagation phase, phase-matching can occur for only short distances where the local pressure reaches the optimum of ~ 15–20 Torr. The resulting pressure peak is shifted to higher pressure by the pressure drop and broadened by the density gradient. In light of these effects, we can see that the primary role of the end sections in the lower-pressure phase-matched regime is to absorb the light generated in the central section.

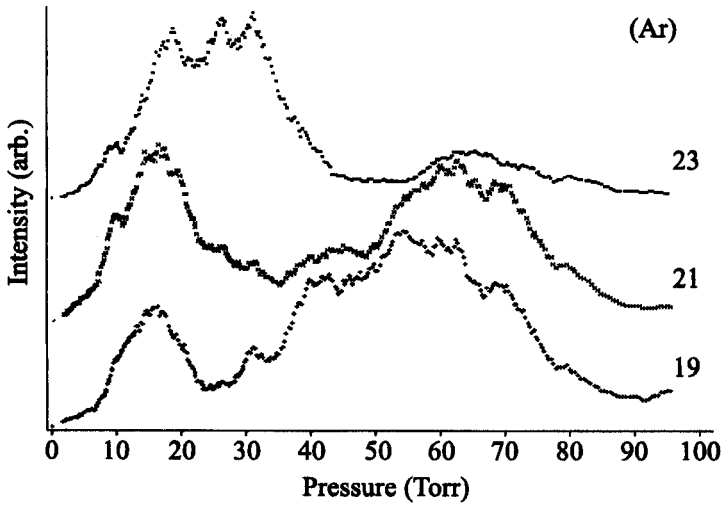

Fig. 11. Pressure dependence of the signal for harmonics 19, 21, 23 generated in argon at a peak intensity of 1.2×10^{14} W/cm^2.

For higher incident intensity, there is another phase-matching regime in which there are two additional contributions to the dispersive phase mismatch. The nonlinear index of refraction and the free electrons generated in the ionization process change the optimum pressure for phase-matching. The latter is particularly important, because high-order harmonic generation requires intensities sufficient for ionization. In general, both of these contributions can influence the propagation of the fundamental, particularly for sufficiently high pressure and/or laser intensity. The effect of the nonlinear index is to increase the index of refraction the neutral gas atoms experienced by the fundamental. While this will change the optimum pressure, it does not play a dominant role in phase-matching. For example in argon, $n_2 I$ is only about 7% of the linear component $N_a \delta$ at an intensity of 2×10^{14} W/cm^2.

This calculation uses a value of $n_2 = 9.8 \times 10^{-24}$ cm^2/W at one bar[56]; experiments on self-phase modulation with femtosecond pulses suggest that n^2 may actually be lower by a factor of 4.[18] In contrast, plasma is strongly dispersive and can strongly limit the harmonic yield. For a plane wave propagating in a plasma electron density of 10^{17}/cm^3, generating a harmonic order of $q = 27$, the coherence length, $l_c = 1/\Delta k$, over which the harmonic phase slips by π from the fundamental due to plasma dispersion, is only 500 μm. An increase in the interaction length beyond this length will never increase the signal, as the output will always emerge only from the last coherence length.

Equation (5) can be rewritten to include the effects of the free-electron density

$$\Delta k \approx q \frac{u_{11}^2 \lambda_1}{4\pi a^2} + N_e r_e (q\lambda_1 - \lambda_q) - \frac{2\pi N_a}{\lambda_q} (\delta(\lambda_1) - \delta(\lambda_q)) . \tag{11}$$

It can easily be seen from Eq. (11) that as N_e increases, the atomic density must also be increased increased to maintain phase-matching. For low ionization fractions η, this may be accomplished by increasing the gas density. Therefore, in general there exists a critical ionization fraction, η_{cr}, dependent on the gas-species, for which the dispersion of the neutrals is balanced by the plasma dispersion.[51] This results in a second regime for phase-matching, which occurs in the presence of a finite amount of ionization, with or without the presence of a waveguide. Physically, this corresponds to the case where the presence of a free-electron plasma increases the phase velocity of the fundamental to greater than c, while the harmonics propagate $\approx c$. Therefore, increased gas pressure (and dispersion) is required to slow down the phase velocity of the fundamental and achieve phase-matching. For plane-wave propagation in Ar and Xe, $\eta_{cr} = 4.8\%$ and 11%, respectively. Fortunately, these estimates of η_{cr} overestimate the effect of ionization by as much as 4–5x because of the modal averaging described above.

We investigated the effects of the neutral and plasma dispersion by measuring the pressure dependence of the harmonics for several gases, xenon, krypton, argon and hydrogen (see Fig. 12(a), respective harmonic orders 23, 25, 29, 25). We performed calculations based on the above considerations to better understand the phase-matching process. In these calculations, we first computed the fractional ionization profile $\eta(r,t)$ using the ADK tunneling ionization rates,[57] then calculated the effective refractive index for each temporal slice of the fundamental using Eq. (10). The harmonic light is generated and propagates in the ionized regions, so we approximate here that it sees the full level of ionization. The pressure dependence of the yield calculated in this manner is shown for the gases in Fig. 12(b). There is very good agreement between the width and locations of the pressure peaks to that found experimentally. A number of conclusions may be drawn from this data. The more dispersive the gas, the lower the optimum pressure, since a lower gas density is required to match the dispersion of the waveguide. The optimum pressure is sensitive to the ionization fraction — the change in η within the pulse causes the pressure peaks to be broadened. For the calculations, the incident intensity was

adjusted downward (by 15–30%) so that ionization did not dominate the phase-matching. This would be experimentally consistent with a slight defocusing of the guided beam. Other uncertainties in the calculation are the exact refractive index of the harmonic and the ionization rate. We estimate that the ionization level at the peak of the pulse was ~6% (Xe and Kr), ~8% (Ar), and 2.6% (H).

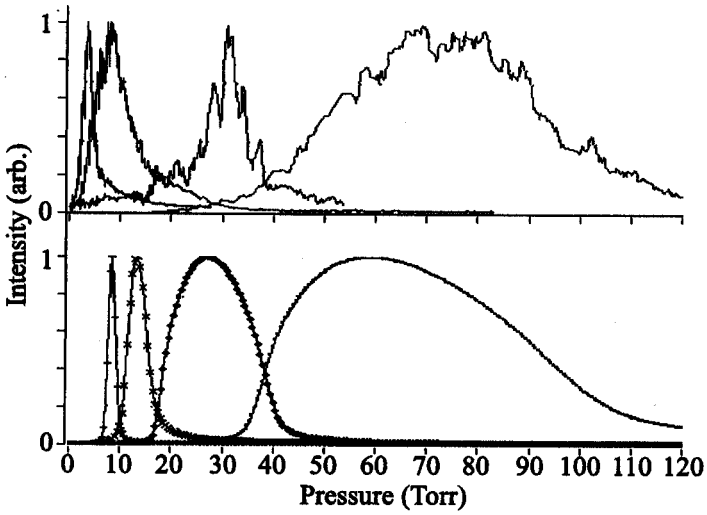

Fig. 12. Measured (a) and calculated (b) pressure dependence of the harmonic yield for several gases. In order of increasing optimum pressure, the curves correspond to Xe, Kr, Ar and H_2 and harmonic orders 23, 25, 29, 25.

The guided wave geometry provides for another very interesting regime of phase-matching. At still higher intensity, the nature of the phase-matching is dominated by the plasma dispersion. For intensities capable of producing the critical ionization fraction η_{cr} at which there is a balance between plasma and atomic dispersion, the optimum yield is extremely sensitive to both the pressure and the ionization level. This is seen clearly in Fig. 13(a), which shows the calculated optimum pressure vs. ionization fraction for argon gas. The rapid variation of the instantaneous intensity that results from the oscillations at the carrier frequency leads to incremental "step" increases in η at each half-cycle of the field. As η approaches η_{cr}, each of these steps should have a distinct optimum pressure (see Fig. 13(a)). Note that the location of these pressure peaks is sensitive to the absolute phase of the carrier to the pulse envelope. Experimentally, the lack of control over this absolute phase leads to rapid fluctuations in the yield at high pressures (see Fig. 13(b)). These absolute phase effects may provide a method of generating efficient attosecond duration XUV pulses from the guided wave geometry, because the phase-matching is optimized only for a small time period within a single cycle of the driving field.

The dependence of the phase-matching on ionization has the important implication that optimum phase-matching is limited to those harmonics that can be

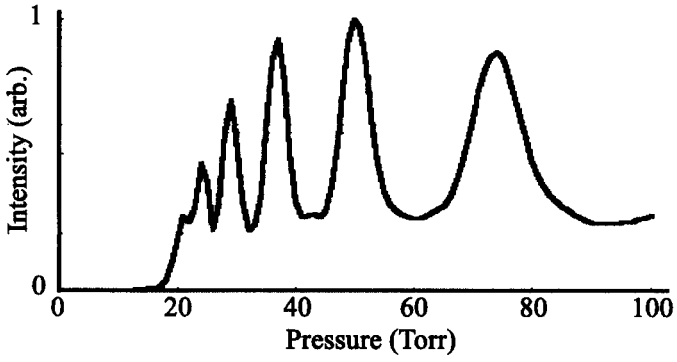

(a)

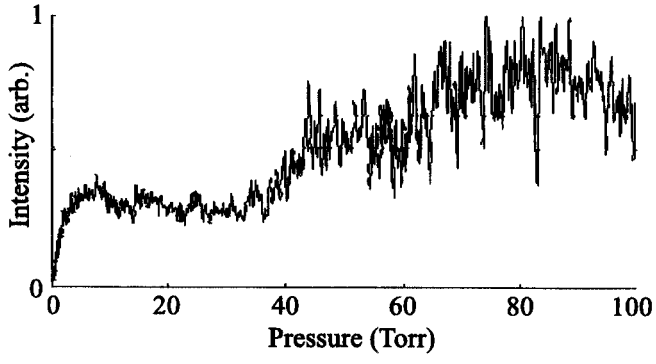

(b)

Fig. 13. (a) Calculated pressure dependence of the yield for high intensity (2.2×10^{14} W/cm^2) in argon; (b) Measured signal at an incident intensity of 4×10^{14} W/cm^2.

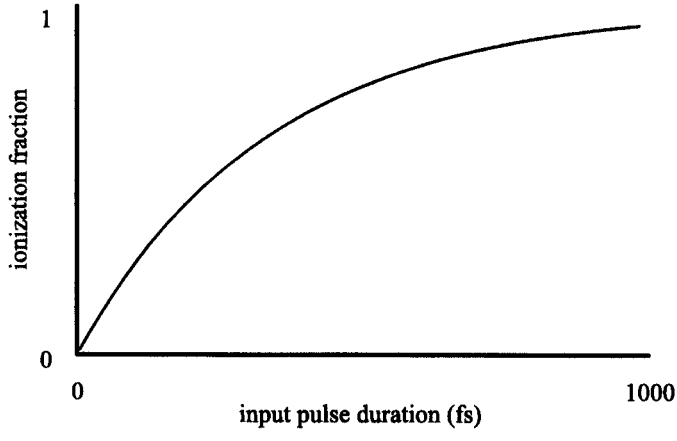

Fig. 14. Calculated ionization fraction at the peak of pulses of varying duration but with equal peak intensity of 1.75×10^{14} W/cm^2, an intensity that corresponds to a cutoff harmonic of order 31 in argon.

generated with ionization levels $< \eta_{cr}$. Since atoms may experience higher intensity at a given level of ionization when irradiated with shorter pulses,[33,39] a short pulse duration is critical in attaining high-order phase-matched harmonics. Figure 14 shows a calculation of the ionization fraction for pulses of the same peak intensity but varying pulse duration. The chosen peak intensity of 1.75×10^{14} W/cm^2 corresponds to a harmonic cutoff of 31st order in argon. Under these conditions, the ionization fraction at the peak of a 200 fs pulse is 40%, while for a 20 fs pulse it is only 6%. Clearly, irradiation with short pulses allows an atom to experience much higher intensity at low fractions of ionization. We see improved yield at harmonics above order 33, though the phase-matching is not as optimal because these harmonics are generated at higher levels of ionization. In our current work, we are exploring the use of still shorter input pulses to further reduce the level of ionization, and the use of high-order frequency mixing to more directly counteract the free electron dispersion.[26,54] Our calculations indicate that η_{cr} increases with every short-wavelength photon in the process. If phase-matching can be reached at full ionization, efficient conversion from ions will be possible, resulting in dramatic increases in both the conversion efficiency and the harmonic photon energy.

5. Conclusions

The use of a capillary to guide the driving pulses during harmonic generation and parametric mixing not only increases the interaction length with the nonlinear medium, but also allows the phase-matching of the process to make use of that increase. We are currently working to further increase the efficiency and wavelength range of the frequency conversion of ultrafast pulses farther into the VUV and EUV. This technique should extend the versatility of table-top ultrafast lasers to enable the investigation of ultrafast phenomena at short wavelengths.

Acknowledgments

The authors gratefully acknowledge support for this work from the National Science Foundation. H. Kapteyn acknowledges support from an Alfred P. Sloan Foundation Fellowship.

References

1. S. Backus, C. Durfee, M. M. Murnane and H. C. Kapteyn, *Rev. Sci. Instrum.* **69**, 1207 (1998).
2. G. Cerullo, M. Nisoli, S. Stagira and S. D. Silvestri, *Opt. Lett.* **23**, 1283 (1998).
3. A. Shirakawa, I. Sakane and T. Kobayashi, *Opt. Lett.* **23**, 1292 (1998).
4. T. Elaesser, J. G. Fujimoto, D. A. Wiersma and W. Zinth, in *Chemical Physics*, eds. F. P. Schafer, J. P. Toennies and W. Zinth (Springer-Verlag, Berlin, 1998), Vol. 63.
5. R. L. Byer, *J. Nonlin. Opt. Phys. Mater.* **6**, 549 (1997).
6. J. Ringling, O. Kittelmann, F. Noack, G. Korn and J. Squier, *Opt. Lett.* **18**, 2035 (1993).
7. S. Backus, J. Peatross, E. Zeek, A. Rundquist, G. Taft, M. M. Murnane and H. C. Kapteyn, *Opt. Lett.* **21**, 665 (1996).

8. J. Young, G. Bjorkland, A. Kung, R. Miles and S. E. Harris, *Phys. Rev. Lett.* **27**, 1551 (1971).
9. A. H. Kung, J. F. Young and S. E. Harris, *Appl. Phys. Lett.* **22**, 301 (1973).
10. J. F. Reintjes, in *Nonlinear Optical Parametric Processes in Liquids and Gases* (Academic Press, 1984).
11. T. Chu, A. Bouvier, A. J. Bouvier and R. Fischer, *J. de Phys. France* **49**, 1725 (1988).
12. J. F. Ward and G. H. C. New, *Phys. Rev.* **185**, 57 (1969).
13. G. C. Bjorklund, *IEEE J. Quant. Elect.* **QE-11**, 287 (1975).
14. C. G. Durfee, S. Backus, M. M. Murnane and H. C. Kapteyn, *Opt. Lett.* **22**, 1565 (1997).
15. G. P. Agrawal, in *Nonlinear Fiber Optics*, 2nd edn. (Academic Press, San Diego, 1995).
16. P. Rabinowitz, A. Kaldor, R. Brickman and W. Schmidt, *Appl. Opt.* **15**, 2005 (1976).
17. M. Nisoli, S. De Silvestri and O. Svelto, *Appl. Phys. Lett.* **68**, 2793 (1996).
18. M. Nisoli, S. D. Silvestri, O. Svelto, R. Szipocs, K. Ferencz, C. Spielmann, S. Sartania and F. Krausz, *Opt. Lett.* **22**, 522 (1997).
19. M. Castillejo, J. Y. Zhou and M. H. R. Hutchinson, *Appl. Phys.* **B45**, 293 (1988).
20. E. A. J. Marcatili and R. A. Schmeltzer, *Bell Syst. Tech. J.* **43**, 1783 (1964).
21. J. J. Degnan, *Appl. Opt.* **12**, 1026 (1973).
22. M. Schnurer, Z. Cheng, S. Sartania, M. Hentschel, G. Tempea, T. Brabec and F. Krausz, *Appl. Phys.* **B67**, 263 (1998).
23. G. Tempea and T. Brabec, *Opt. Lett.* **23**, 762 (1998).
24. A. E. Siegman, *Lasers* (University Science Books, Mill Valley, 1986).
25. R. H. Stolen and J. E. Bjorkholm, *IEEE J. Quant. Elect.* **QE-18**, 1062 (1982).
26. H. Milchberg, C. G. Durfee III and T. McIlrath, *Phys. Rev. Lett.* **75**, 2494 (1995).
27. V. G. Arkhipkin, Y. I. Heller, A. K. Popov and A. S. Provorov, *Appl. Phys.* **B37**, 93 (1985).
28. C. G. Durfee, S. Backus, M. M. Murnane and H. C. Kapteyn, in *Applications of High Field and Short wavelength Sources*, eds. L. DiMauro, M. M. Murnane and A. l'Huillier (Plenum, New York, 1998).
29. S. Backus, C. Durfee, G. Mourou, H. C. Kapteyn and M. M. Murnane, *Opt. Lett.* **22**, 1256 (1997).
30. A. Dalgarno and A. E. Kingston, *Proc. Roy. Soc.* **A259**, 424 (1966).
31. C. G. Durfee, S. Backus, H. C. Kapteyn and M. M. Murnane, *Opt. Lett.*, to be published (1999).
32. A. L'Huillier and P. Balcou, *Phys. Rev. Lett.* **70**, 774 (1993).
33. J. Zhou, J. Peatross, M. M. Murnane, H. C. Kapteyn and I. P. Christov, *Phys. Rev. Lett.* **76**, 752 (1996).
34. A. McPherson, G. Gibson, H. Jara, U. Johann, T. S. Luk, I. A. McIntyre, K. Boyer and C. K. Rhodes, *J. Opt. Soc. Am.* **B4**, 595 (1987).
35. A. L'Huillier, K. J. Schafer and K. C. Kulander, *Phys. Rev. Lett.* **66**, 2200 (1991).
36. M. Lewenstein, P. Balcou, M. Y. Ivanov and P. B. Corkum, *Phys. Rev.* **A49**, 2117 (1993).
37. K. C. Kulander, K. J. Schafer and J. L. Krause, in *NATO 3rd Conference on Super Intense Laser-Atom Physics* (Han-sur-Lesse, Belgium, 1993).
38. J. J. Macklin, J. D. Kmetec and C. L. Gordon, III, *Phys. Rev. Lett.* **70**, 766 (1993).
39. I. P. Christov, J. P. Zhou, J. Peatross, A. Rundquist, M. M. Murnane and H. C. Kapteyn, *Phys. Rev. Lett.* **77**, 1743 (1996).
40. I. P. Christov, M. M. Murnane and H. C. Kapteyn, *Phys. Rev. Lett.* **78**, 1251 (1997).
41. Z. Chang, A. Rundquist, H. Wang, H. C. Kapteyn and M. M. Murnane, *Phys. Rev. Lett.* **79**, 2967 (1997).

42. C. Spielmann *et al.*, *Science* **278**, 661 (1997).
43. P. B. Corkum, N. H. Burnett and M. Y. Ivanov, *Opt. Lett.* **19**, 1870 (1994).
44. P. Antoine *et al.*, *Phys. Rev.* **A56**, 4960 (1997).
45. A. L'Huillier, X. Li and L. Lompre, *J. Opt. Soc. Am.* **B7**, 527 (1990).
46. T. D. Donnelly, T. Ditmire, K. Neumann, M. D. Perry and R. W. Falcone, *Phys. Rev. Lett.* **76**, 2472 (1996).
47. M. B. Gaarde, P. Antoine, A. L'Huillier, K. J. Shafer and K. C. Kulander, *Phys. Rev.* **A57**, 4553 (1998).
48. P. Salieres, A. L'Huillier and M. Lewenstein, *Phys. Rev. Lett.* **74**, 3776 (1995).
49. A. Rundquist, C. G. Durfee, Z. Chang, C. Herne, S. Backus, M. M. Murnane and H. C. Kapteyn, *Science* **280**, 1412 (1998).
50. C. G. Durfee, A. Rundquist, S. Backus, C. Herne, M. M. Murnane and H. C. Kapteyn, *Phys. Rev. Lett.*, submitted (1999).
51. A. Rundquist, PhD Thesis (Washington State University, Pullman, 1998).
52. E. Constant, D. Garzella, P. Breger, E. Meval, C. Dorrer, C. LeBlanc, F. Salin and P. Agostini, *Phys. Rev. Lett.* **82**, 1668 (1999).
53. I. P. Christov, H. C. Kapteyn and M. M. Murnane, *Opt. Expr.* **3**, 360 (1998).
54. P. L. Shkolnikov, A. E. Kaplan and A. Lago, *Opt. Lett.* **18**, 1700 (1993).
55. D. J. Santeler, *J. Vac. Sci. Tech.* **A4**, 348 (1986).
56. H. J. Lehmeier, W. Leupacher and A. Penzkofer, *Opt. Commun.* **56**, 67 (1985).
57. M. V. Ammosov, N. B. Delone and V. P. Krainov, *Sov. Phys. JETP* **64**, 1191 (1986).